

# Bare versus Insulated Conductors for Improving the Lightning Response of Interconnected Wind Turbine Grounding Systems

R. Alipio, A. De Conti, N. Duarte, and M. T. Correia de Barros

**Abstract--** This paper investigates the lightning response of a pair of interconnected wind turbine grounding systems assuming their connection to be performed by a bare or insulated underground conductor. Typical first and subsequent stroke current waveforms are injected at one of the grounding systems and the transient response is studied for different soil resistivities considering frequency-dependent soil parameters. The ground potential rise (GPR) at the current injection point and the voltages transferred to the adjacent grounding system are calculated. GPR peak reductions are obtained using either a bare or insulated conductor, but the former is more effective. It is shown that when the wind turbine grounding systems are interconnected by a bare conductor, the GPR peak reduction is essentially due to the interconnecting wire. On the other hand, when the interconnection is made through an insulated conductor, the GPR reduction is related to the current that is partly diverted to the adjacent tower, especially for high resistivity soils. For an insulated interconnecting conductor and first lightning return-stroke currents, the adjacent grounding system also contributes to the GPR peak decrease.

**Keywords:** wind turbines, lightning transients, grounding, bare conductor, insulated conductor.

## I. INTRODUCTION

WIND energy is one of the fastest growing renewable energy technologies [1]. Due to economic and technical reasons, modern wind turbines (WTs) are preferably installed in high-wind sites such as coastal areas, hilltops or mountain ridges [2], [3]. Such locations are likely to have high lightning occurrence. Also, the heights of wind turbines have been constantly increasing over the years and as a result they have become more vulnerable to lightning [2], [4]. According with [3], up to 50% of all events related to lightning strikes in wind

farms cause damage to control systems and sensitive electronic equipment. These aspects make the design of a proper lightning protection system, which includes the grounding system, of high importance.

To limit the ground potential rise (GPR) due to lightning strikes to wind turbines, a suitable low-impedance earth termination system is needed. The main factor that contributes to the reduction of the grounding impedance is the increase of the area covered by the grounding electrodes. For such, IEC standard TR61400-24 recommends the interconnection of the grounding systems of each individual wind turbine of the farm [2]. This leads to a strong reduction of the dc grounding resistance seen by each individual wind turbine, but may not lead to a similar improvement in their lightning performance.

Much work has been done lately on the lightning response of wind turbines [5]–[10], including investigations on the interconnection of adjacent wind turbine grounding systems [11]–[14]. A common conclusion is that the GPR reduction observed in a pair of interconnected wind turbine grounding systems struck by lightning is essentially due to the effect of the interconnecting conductor, if it is bare. In this case, the adjacent WT would only modify the late-time response of the GPR because the effective length of the interconnecting conductor is usually shorter than the typical distance between wind turbines. However, as suggested in [13], in some cases it may be preferable to perform the connection using an insulated conductor. This would contribute to mitigate electromagnetic compatibility issues and reduce step voltages, thus improving the safety of equipment and personnel. Nevertheless, no results were presented in [13] considering this idea. For this reason, it is important to assess and compare the lightning performance of wind turbine grounding systems connected through bare or insulated conductors. This paper aims to clarify this issue by presenting simulation results obtained with an approach based on the combined use of a numerical electromagnetic model with transmission line theory, considering frequency-dependent soil parameters.

This paper is organized as follows. Section II presents the simulated system. Modeling details are presented in Section III. Results and analyses are presented in Section IV, followed by conclusions in Section V.

## II. GROUNDING SYSTEM GEOMETRY

The geometry of each wind turbine grounding system considered in this paper is shown in Fig. 1(a). It consists of five conducting rings and eight bonding conductors, all part of

---

This paper was supported by the National Council for Scientific and Technological Development (CNPq) under grants 312763/2018-2 and 306006/2019-7.

R. Alipio is with the Department of Electrical Engineering of Federal Center of Technological Education (CEFET-MG), Belo Horizonte, MG, Brazil (e-mail of corresponding author: rafael.alipio@cefetmg.br).

A. De Conti is with the Department of Electrical Engineering, Universidade Federal de Minas Gerais (UFMG), Belo Horizonte, Brazil (e-mail: conti@cpdee.ufmg.br).

N. Duarte is with the Graduate Program of Electrical Engineering (PPGEE), Universidade Federal de Minas Gerais (UFMG), Belo Horizonte, Brazil (e-mail: naiara.duarte@gmail.com)

M. T. Correia De Barros is with Instituto Superior Técnico (IST), University of Lisbon (UL), Lisbon, Portugal (e-mail: teresa.correiaedebarras@tecnico.ulisboa.pt).

Paper submitted to the International Conference on Power Systems Transients (IPST2020) in Belo Horizonte, Brazil June 6-10, 2021.

the tower foundation. Two grounding systems like this are connected through a bare or insulated conductor buried at 0.5 m depth, as shown in Fig. 1(b). The bare conductors are assumed perfectly conducting with 7-mm radius and the insulated conductor has inner and outer radius of 5.8 mm and 7.6 mm, respectively, and insulation constant dielectric of 2.3. **Three different lengths  $L$  of interconnecting conductor are assumed in this paper, namely 100 m, 200 m and 300, in order to cover from small to large wind farms.**

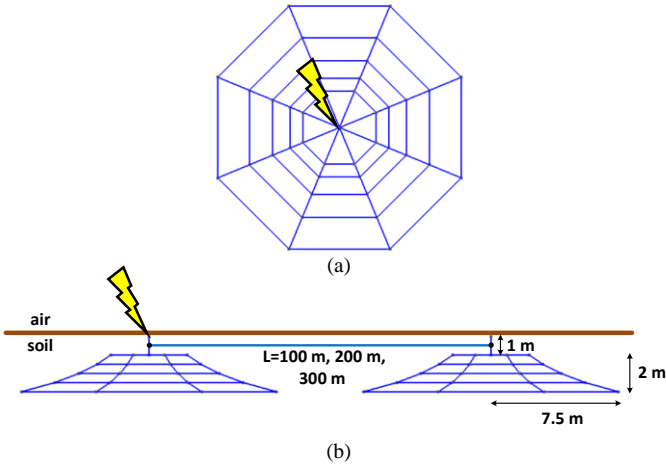


Fig. 1. (a) Single wind turbine grounding system (upper view), and (b) interconnected wind turbine grounding systems (lateral view).

### III. MODELING GUIDELINES

#### A. Frequency Dependence of Soil Electrical Parameters

Several experimentally-obtained formulas for modeling the frequency dependence of soil parameters have been proposed in the literature. In this paper, the Alipio-Visacro model [15] is considered, which is based on the measured frequency response of 65 different types of soils with low-frequency resistivity values ( $\rho_0$ ) ranging from 60 to 18,000  $\Omega\text{m}$ . This model satisfies causality and is recommended by CIGRÉ [16] for lightning-related studies. It states that soil resistivity,  $\rho_g(f)$ , and permittivity,  $\epsilon_g(f)$ , can be calculated at a given frequency  $f$  (Hz) by using:

$$\rho_g(f) = \rho_0 \{1 + 4.7 \times 10^{-6} \times \rho_0^{0.73} \times f^{0.54}\}^{-1} \quad (\Omega\text{m}) \quad (1)$$

$$\epsilon_g(f) = 9.5\epsilon_0 \times 10^4 \times \sigma_0^{0.27} \times f^{-0.46} + 12\epsilon_0 \quad (\text{F/m}) \quad (2)$$

where  $\epsilon_0$  is the vacuum permittivity and  $\sigma_0 = 1/\rho_0$  is the low-frequency soil conductivity.

#### B. Lightning Current Waveforms

In order to consider both fast- and slow-front lightning currents, typical first and subsequent stroke current waveforms are used in the simulations. These waveforms, which are shown in Fig. 2, are modeled as the sum of Heidler's functions as detailed in [17]. They reproduce the median parameters of downward negative lightning measured at Mount San Salvatore [18]. The first-stroke current is characterized by a peak value of 31 kA and a virtual front time (calculated as the

time between 30% and 90% of its peak value, divided by 0.6 [17]) of 3.8  $\mu\text{s}$ , whereas the subsequent stroke current has a peak value of 12 kA and a virtual front time of 0.67  $\mu\text{s}$ . **The time-to-half-peak is 75  $\mu\text{s}$  for first stroke currents, and 50  $\mu\text{s}$  for subsequent strokes.**

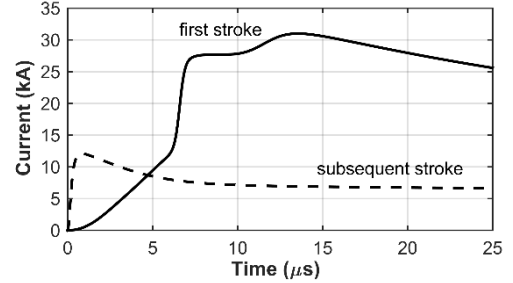


Fig. 2. Return-stroke currents used in the simulations.

#### C. Wind Farm Grounding System

In this paper, a nodal-type formulation similar to the one proposed in [19] is used to simulate the wind farm grounding system shown in Fig. 1 in the frequency domain. The final solution of the model is expressed as

$$\mathbf{Y}_G \cdot \mathbf{U} = \mathbf{I}_E \quad (3)$$

where  $\mathbf{U}$  is the vector of nodal voltages,  $\mathbf{I}_E$  is the vector of injected currents, and  $\mathbf{Y}_G$  is the global grounding admittance matrix, which expresses both the electromagnetic coupling between the grounding system elements and the circuit connectivity. Taking as reference Fig. 1, matrix  $\mathbf{Y}_G$  describes each grounding system and their interconnecting conductor.

The wind turbine grounding systems and the bare interconnecting conductor were modeled as cylindrical conductors using the hybrid electromagnetic model (HEM), which solves Maxwell's equations numerically via the vector and scalar potentials using the thin wire approximation [20]. On the other hand, the insulated conductor was modeled using transmission line theory. The per-unit-length parameter calculation was performed as in [21], except that the earth return impedance expression of Sunde [22] was considered to include ground displacement currents, as well as the variation of  $\rho_g$  and  $\epsilon_g$  with frequency. The ground admittance is determined from the earth return impedance and the ground propagation constant as in [23]. The resulting model is shown in [24] to represent the transient response of underground conductors in good agreement with the rigorous full-wave finite-difference time-domain (FDTD) method. Details about the per-unit-length parameter calculation are given in Appendix. The insulated conductor is then represented by the nodal admittance matrix [25]

$$\mathbf{Y}_{ins} = \begin{bmatrix} Y_c(1+A^2)(1-A^2)^{-1} & -2Y_c A(1-A^2)^{-1} \\ -2Y_c A(1-A^2)^{-1} & Y_c(1+A^2)(1-A^2)^{-1} \end{bmatrix} \quad (4)$$

where  $Y_c$  is the characteristic admittance and  $A$  is the propagation function, calculated as

$$Y_c = \sqrt{Y/Z} \quad (5)$$

$$A = \exp(-\ell\sqrt{ZY}) \quad (6)$$

In (5) and (6),  $\ell$  is the conductor length, and  $Z$  and  $Y$  are respectively the per-unit-length impedance and admittance of the insulated conductor (see Appendix).  $Y_{ins}$  can be easily accommodated in the global admittance matrix  $Y_G$ , allowing the simulation of the system shown in Fig. 1(b) assuming the interconnecting conductor to be insulated.

In this paper, a harmonic current of 1 A is injected at the center of one of the WT grounding systems as shown in Fig. 1(a) and the system of equations (3) is solved at a set of frequencies in order to determine the voltage  $U_k(j\omega)$  at the  $k$ -th system node. If  $k$  is the current injection node, the grounding impedance is then calculated as

$$Z(j\omega) = \frac{U_k(j\omega)}{1 \text{ A}} \quad (7)$$

Finally, the time domain voltage  $u_k(t)$  at the  $k$ -th system node can be calculated as

$$u_k(t) = \mathfrak{F}^{-1}\{U_k(j\omega)\mathfrak{F}[i(t)]\} \quad (8)$$

where  $\mathfrak{F}$  and  $\mathfrak{F}^{-1}$  denote the Fourier and inverse Fourier transforms, respectively.

#### IV. RESULTS

This section presents simulation results of the lightning response of the interconnected wind turbine grounding systems of Fig. 1, both in frequency and time domains, comparing their performance for different connection types.

##### A. Propagation Characteristics of the Interconnecting Conductors

Fig. 3 shows the attenuation constant  $\alpha$  associated with the bare and insulated conductors for two values of soil resistivity ( $300 \Omega\text{m}$  and  $3000 \Omega\text{m}$ ). This parameter, calculated as the real part of  $\sqrt{ZY}$  [25], increases with increasing frequency. Also, its value is greater for low-resistivity soils and for the bare conductor. This means that if a bare conductor is used to connect the wind turbine grounding systems, only part of the interconnecting conductor will be effectively seen by the propagating current, which will be strongly drained to soil near the current injection point. This is expressed by the effective length concept that is useful in the transient analysis of grounding systems. For the insulated conductor, the current is not directly drained to the soil. However, part of it is used to charge the capacitance associated with the insulation. Along with ground and conductor losses, this contributes to increasing the attenuation in the high-frequency range.

Fig. 4 shows the phase velocity  $v_{ph}$  associated with the bare and insulated conductors, calculated as the angular frequency  $\omega$  divided by the imaginary part of  $\sqrt{ZY}$ . This parameter is greater for the insulated conductor than for the bare conductor in the whole frequency range, but the differences are more significant up to tens of kHz, where  $v_{ph}$  associated with the insulated conductor is nearly insensitive to the soil resistivity. At higher frequencies, this behavior changes and the propagation velocity associated with the insulated conductor starts to increase with increasing soil

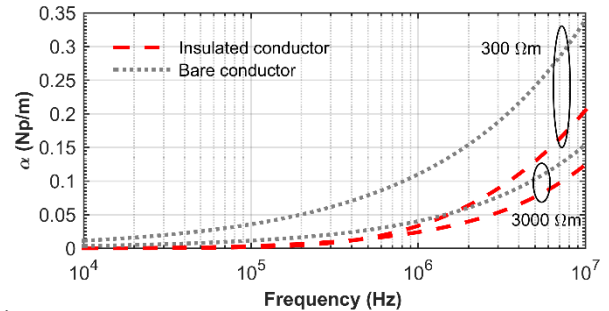


Fig. 3. Attenuation constant associated with the bare and insulated conductors that connect the grounding systems, for  $300 \Omega\text{m}$  and  $3000 \Omega\text{m}$  soils.

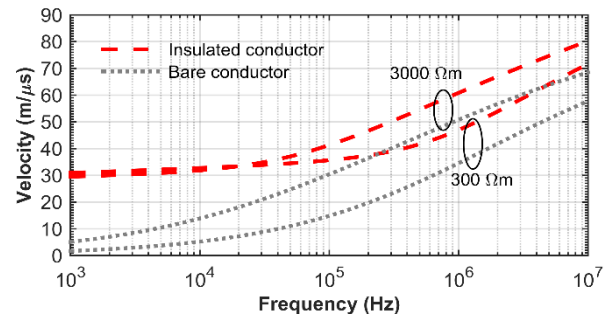


Fig. 4. Phase velocity associated with the bare and insulated conductors that connect the grounding systems, for  $300 \Omega\text{m}$  and  $3000 \Omega\text{m}$  soils.

resistivity, similarly as observed with the bare wire in the whole frequency range. The dependence of  $v_{ph}$  on the soil resistivity can be explained by the fact that the electromagnetic properties of soil gradually approach that of a perfect dielectric as the soil conductivity is reduced. If either the soil resistivity or the frequency approaches infinity, the velocity associated with the bare conductor approaches the upper limit given by  $c/\sqrt{\epsilon_{rg}}$ , where  $c$  is the speed of light and  $\epsilon_{rg}$  is the soil relative permittivity. For the insulated conductor, the equivalent permittivity is reduced due to the influence of the insulation, which usually has a relative permittivity lower than that of the soil, and this upper limit is increased.

Overall, the reduced attenuation and the higher propagation velocity associated with the insulated conductor in the frequency range associated with lightning currents are likely to increase the influence of the adjacent grounding system on the transient behavior of the wind turbine struck by lightning. This happens because reflected waves coming from the adjacent grounding system are expected to have greater magnitudes and to arrive faster at the current injection point than for a bare conductor. This is confirmed in the transient analysis presented in section IV-C.

##### B. Harmonic Grounding Impedance

Fig. 5 shows the harmonic grounding impedance calculated by (7) for four different values of soil resistivity ( $100$ ,  $300$ ,  $1000$  and  $3000 \Omega\text{m}$ ) and three different grounding configurations. The case labeled as “single WT” is used as reference and corresponds to the grounding system of a single wind turbine. The other two cases, labeled as “2 WTs (bare conductor)” and “2 WTs (insulated conductor)”, correspond to the configuration shown in Fig. 1(b), in which the adjacent

wind turbine grounding system is also included, and the two grounding systems are connected either through a 100-m or 300-m bare or insulated conductor.

The harmonic grounding impedance is seen to depend on soil resistivity, frequency range, interconnection type and length of the interconnecting conductor. As expected, the adjacent grounding system leads to a significant reduction of the harmonic impedance in the low-frequency range, which can be seen by comparing the curves corresponding to the interconnected grounding system with those labeled as “single WT”. The reduction is stronger if the interconnection is performed by a bare conductor since the conductor itself contributes to the current injected into the soil. In this case, the low-frequency impedance is reduced by 69% and 81%, respectively for the 100-m and 300-m interconnecting conductor, regardless of the soil resistivity. For the insulated conductor, this reduction is limited to 50%.

As the frequency increases, the effect of the adjacent tower becomes gradually negligible and the grounding impedance corresponding to the interconnected systems shows a behavior that is similar to that of the single wind turbine. This similarity, which is observed regardless of the interconnection type, indicates that above several hundreds of kHz the equivalent grounding impedance is practically determined by the frequency response of the wind turbine struck by lightning. The critical frequency at which this occurs is higher for the interconnection through a bare conductor, especially for low-resistivity soils. This is related to the contribution of the bare conductor to the current injected into the soil, which remains significant even at frequencies in which the adjacent grounding system no longer contributes to reducing the grounding impedance. It is also seen that the frequency at which the curves associated with the two interconnected WTs start to move towards that associated with a single turbine is lower for the longer distance between the turbines, for both bare and insulated interconnecting conductors. The current injected into the soil by the bare conductor also explains the impedance differences observed in the upper frequency limit, in which the impedance magnitude is reduced compared to that of a single wind turbine. In the case of the insulated conductor, the impedance reduction observed in the upper frequency limit is related to the current required to charge the insulation capacitance.

#### A. Ground Potential Rise (GPR)

Figs. 6, 7 and 8 show the GPR at the current injection point caused by the first stroke current of Fig. 2 assuming the interconnection between the adjacent wind turbine grounding systems to be performed by a bare or insulated conductor for 100, 300, 1000 and 3000- $\Omega$ m soils, respectively for distances between WTs of 100 m, 200 m and 300 m. For comparison purposes, the transient performance of a single wind turbine grounding system is also included in the figure.

It is observed in Fig. 6 that the interconnection of the grounding systems leads to a GPR reduction that is dependent on soil resistivity, type of interconnecting conductor and distance between WTs. If the interconnection is made through

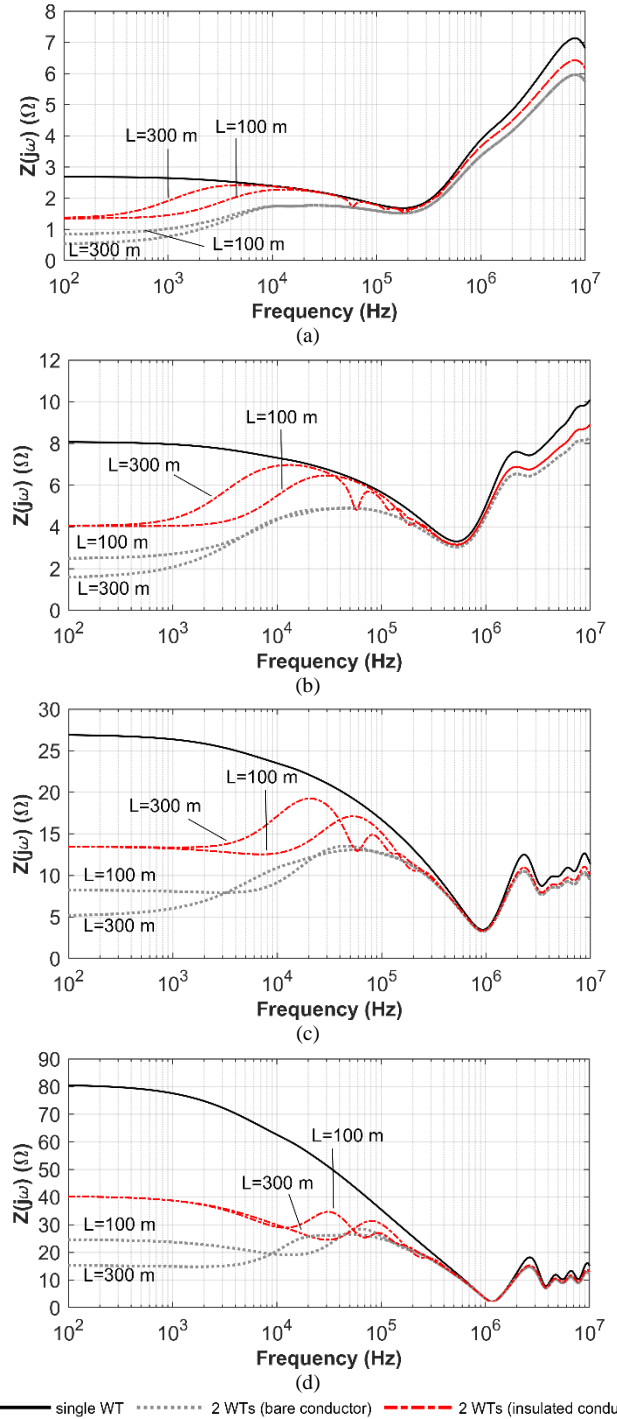


Fig. 5. Harmonic grounding impedance: (a) 100  $\Omega$ m, (b) 300  $\Omega$ m, (c) 1000  $\Omega$ m, and (d) 3000  $\Omega$ m. Two distances are assumed between WTs: 100 m and 300 m.

a bare conductor, two main reasons lead to the GPR reduction. First, the conductor itself contributes to the current injection into the soil up to its effective length. In the investigated conditions, this is the main cause of reduction of the GPR peak, which is in line with the conclusions of [13] and [14]. Larger reductions are observed for higher resistivity soils because the effective length is longer in these cases [26]. Second, the adjacent grounding system reduces the low-frequency grounding impedance seen at the current injection point, which modifies the GPR tail.

If the interconnection is made through an insulated conductor, the conductor itself no longer contributes to the current injection into the soil. Therefore, the GPR reduction mechanism is not the same as in the case of a bare conductor. One of the mechanisms leading to the GPR reduction is the current division path provided by the insulated conductor. This effect is stronger for high-resistivity soils because in this case a larger fraction of the injected current is initially diverted to the insulated conductor. Also, part of the current that is diverted to the insulated conductor is used to charge the insulation capacitance. Such charging process enhances the capacitive effect of the whole grounding system and improves its performance especially for high-resistivity soils. A second effect that contributes to the GPR reduction is the influence of the adjacent grounding system, which is stronger than for the bare conductor. This stems from the fact that the propagating waves travel faster and are less attenuated for an insulated conductor than for a bare conductor, as shown in section IV-A. Therefore, the reflected voltage wave coming from the adjacent grounding system reaches the wind turbine struck by lightning before the GPR peak has been reached, **especially for shorter distances between adjacent WTs**. Also, the transient waves that propagate along the insulated conductor are less attenuated, which enhances the effect of the adjacent grounding. As expected, the adjacent grounding is also responsible for a reduction of the GPR tail similarly as observed if the interconnecting conductor is bare.

Table I summarizes the GPR peak reductions obtained using either a bare or insulated interconnecting conductor for the first stroke current, **in comparison with the single wind turbine**. Both types of interconnection lead to a GPR peak reduction, although the bare conductor is more efficient. **It is seen that increasing the interconnecting bare conductor from 100 m to 300 m does not lead to an additional decrease in the GPR peak, regardless of the soil resistivity. This occurs because even for the higher resistivity soil of 3000  $\Omega\text{m}$ , the effective length considering first stroke currents are expected to be no longer than 100 m [27]. Thus, although the increase of the bare conductor leads to additional reductions of the GPR tail at later times, its peak is not modified. For the interconnecting insulated conductor, a decrease in the percentage reduction of the GPR peak is observed with the increase of the distance between the WTs, mainly for the lower resistivity soils. This stems from the fact that, by increasing this distance, the favorable effect of the reflection coming from the adjacent WT is more attenuated and takes longer to travel forth and back, reaching the struck tower closer to the GPR peak occurrence. The reduction of the effect of the adjacent turbine with the increase of the insulated conductor length is more pronounced for lower resistivity soils, since in this case the wave is more attenuated and propagates more slowly. Also, the most significant loss of efficiency in the GPR peak reduction occurs when the separation between the WTs increases from 100 m to 200 m. For a separation increase from 200 m to 300 m the effect of the adjacent turbine is already too limited. Finally, it is noted that the differences between the GPR reductions obtained**

using bare or insulated conductors tend to decrease with increasing the soil resistivity. This occurs because for higher resistivity soils a large portion of the injected current is diverted to the adjacent tower through the insulated conductor, thus improving its efficiency in decreasing the GPR peak.

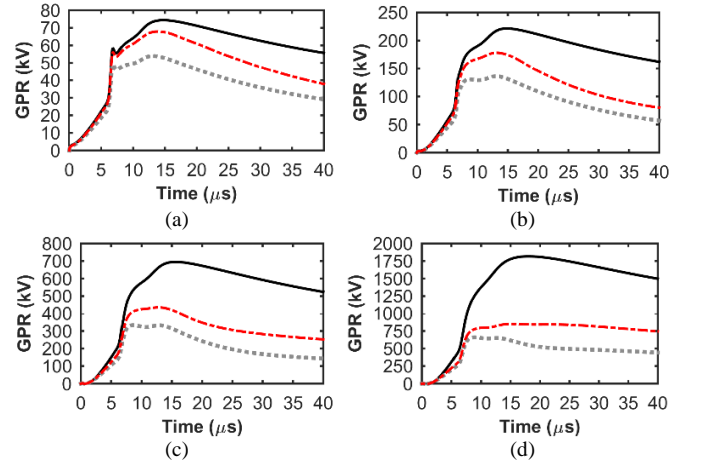


Fig. 6. GPR at the current injection point in response to first strokes, assuming the interconnection by a bare or insulated conductor **and 100 m between WTs**, for different soil resistivity values: (a) 100  $\Omega\text{m}$ , (b) 300  $\Omega\text{m}$ , (c) 1000  $\Omega\text{m}$ , and (d) 3000  $\Omega\text{m}$ . The GPR of a single grounding system is also included for comparison.

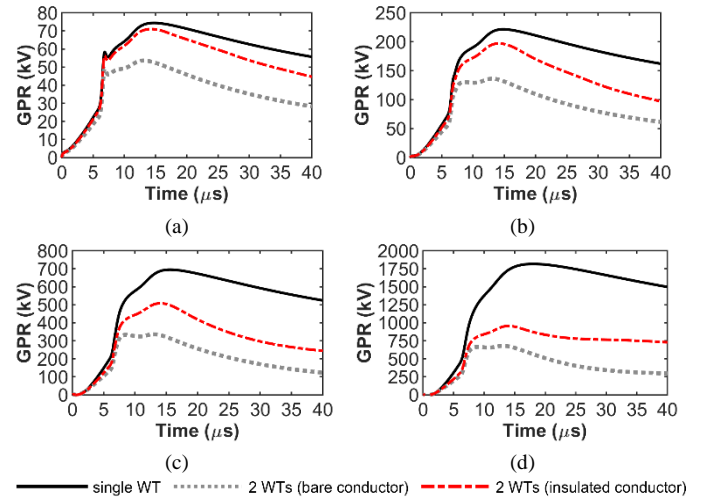


Fig. 7. Same as Fig. 6, but assuming a distance of 200 m between WTs.

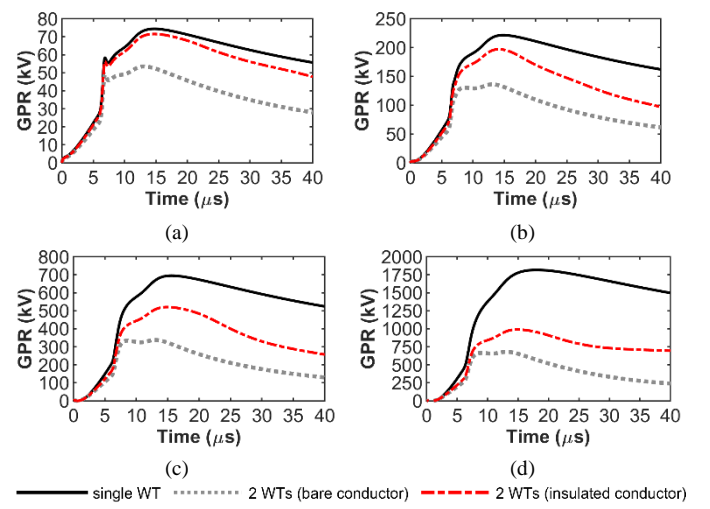


Fig. 8. Same as Fig. 6, but assuming a distance of 300 m between WTs.

TABLE I – GPR PEAK REDUCTIONS FOR FIRST STROKE CURRENTS ASSUMING BARE ( $\Delta_{bare}$ ) OR INSULATED ( $\Delta_{insu}$ ) CONDUCTORS, AND DIFFERENT DISTANCES BETWEEN WTS.

$\rho$ ( $\Omega\text{m}$ )	$L = 100$ m		$L = 200$ m		$L = 300$ m	
	$\Delta_{bare}$ (%)	$\Delta_{insu}$ (%)	$\Delta_{bare}$ (%)	$\Delta_{insu}$ (%)	$\Delta_{bare}$ (%)	$\Delta_{insu}$ (%)
100	27.8	8.7	27.8	4.6	27.8	3.9
300	38.6	19.5	38.6	11.1	38.6	9.9
1000	51.7	37.5	51.7	26.9	51.7	25.1
3000	62.9	53.3	62.9	47.4	62.9	45.5

The previous analysis is now repeated considering the subsequent stroke current of Fig. 2. The results are shown in Figs. 9, 10 and 11, respectively for distances between WTs of 100 m, 200 m and 300 m. Considering the results obtained for the bare conductor, once again the GPR reduction is basically due to the current that is injected into to the soil. Reductions of 12.5% 22.7%, 32.0% and 43.7% are observed in the GPR peaks for the 100, 300, 1000 and 3000- $\Omega\text{m}$  soils, respectively, regardless of the length of the interconnecting bare conductor. These reductions are not as large as those previously observed for first stroke currents because the effective length of the bare conductor is shorter for subsequent strokes due to their higher frequency content [26]. Again, no further reductions in the GPR peak are observed with the increase in the length of the bare interconnection conductor since the effective length for the considered soil resistivities is shorter than 100 m for subsequent strokes [27]. In fact, the effective length for the 3000- $\Omega\text{m}$  soil is around 50 m.

Now considering the results shown in Figs. 9, 10 and 11 for the interconnection made through an insulated conductor, reductions of 4.1% 8.8%, 21.1% and 36.6% are observed in the GPR peak for the 100, 300, 1000 and 3000- $\Omega\text{m}$  soils, respectively, in comparison with the single wind turbine. Differently from the case of first stroke currents, such reductions do not depend on the distance between WTs. As opposed to the behavior observed for a bare conductor, if an insulated conductor is used the adjacent grounding system is likely to have an influence not only on the GPR tail at the lightning-struck tower, but also on the first few microseconds of the transient, mainly for shorter distances between WTs. However, due to the short front-time of the subsequent stroke current and the distance between the wind turbines, the adjacent grounding system is not able to reduce the GPR peak. Thus, for subsequent strokes, the current division path provided by the insulated conductor is the main factor that contributes to the GPR peak reduction. This explains why, unlike the first strokes, the reduction in the GPR peak does not change with the variation in the distance between the WTs. However, it should be emphasized that the shorter this distance, the stronger the influence of the adjacent turbine on reducing the GPR immediately after its peak has been reached. This can be clearly seen comparing, for a given soil resistivity, the red dotted curves of Figs. 9, 10 and 11.

Table II summarizes the GPR peak reductions obtained for the bare and insulated interconnecting conductors assuming the subsequent stroke current. This table does not differentiate with respect to the distance between the WTs since for the subsequent strokes because such distance has no influence on

the percentage reductions in the GPR. Similar to the case of first strokes, the bare conductor is more efficient than the insulated conductor, although the effectiveness of the later tends to improve with increasing the soil resistivity.

Finally, it is worth mentioning that the use of insulated conductors to interconnect WTs grounding systems in a wind farm is a solution normally adopted in specific cases, for instance, to mitigate problems related to interferences in sensitive equipment placed near the interconnecting conductor or to reduce step voltages along the wind farm. Such cables, however, can be subjected to severe lightning surges, as shown in this section, especially in wind farms installed on poor conducting soils. Thus, in the cable design special attention should be given to the insulation requirements to prevent its damage. Eventually, surge arresters at the cable ends may be necessary.

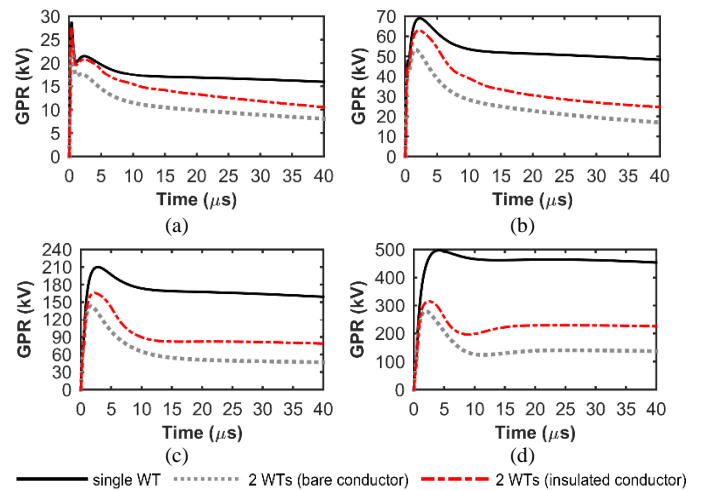


Fig. 9. GPR at the current injection point in response to subsequent strokes, assuming the interconnection by a bare or insulated conductor and 100 m between WTs, for different soil resistivity values: (a) 100  $\Omega\text{m}$ , (b) 300  $\Omega\text{m}$ , (c) 1000  $\Omega\text{m}$ , and (d) 3000  $\Omega\text{m}$ . The GPR of a single grounding system is also included for comparison.

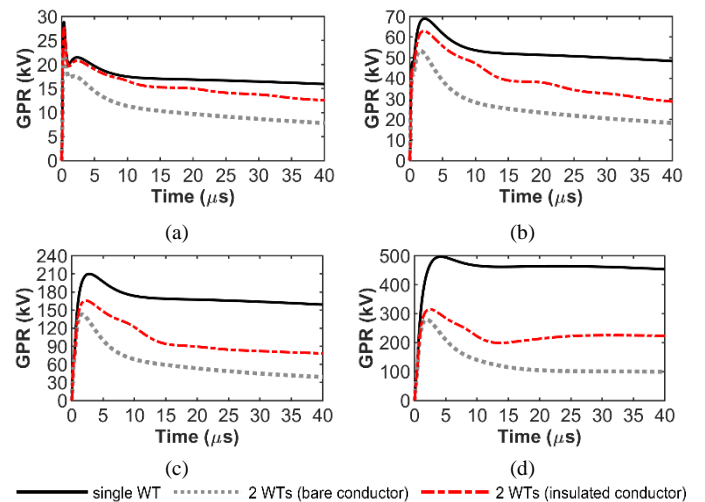


Fig. 10. Same as Fig. 9, but assuming a distance of 200 m between WTs.

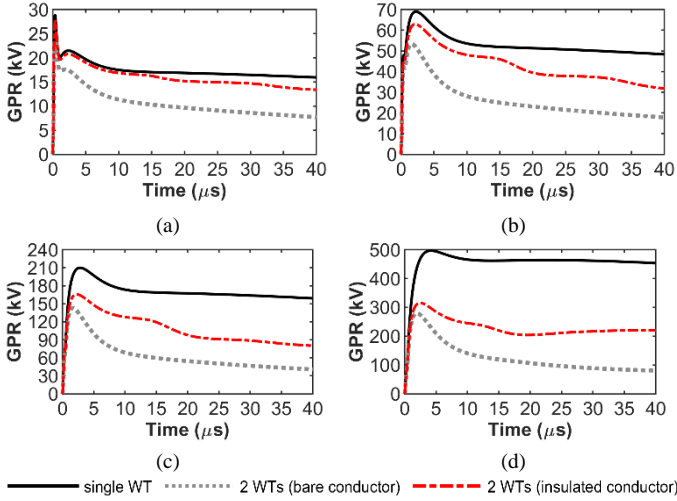


Fig. 11. Same as Fig. 9, but assuming a distance of 300 m between WTs.

TABLE II – GPR PEAK REDUCTIONS FOR SUBSEQUENT STROKE CURRENTS ASSUMING BARE ( $\Delta_{bare}$ ) OR INSULATED ( $\Delta_{insu}$ ) CONDUCTORS.

$\rho$ ( $\Omega\text{m}$ )	$\Delta_{bare}$ (%)	$\Delta_{insu}$ (%)
100	12.5	4.1
300	22.7	8.8
1000	32.0	21.1
3000	43.7	36.6

## V. CONCLUSIONS

This paper assesses the lightning response of two wind turbine grounding systems interconnected through a bare or insulated conductor. Simulations were performed combining an accurate electromagnetic model with transmission line theory, considering frequency-dependent soil parameters. The main conclusions of the paper are summarized below.

- The interconnection between the grounding systems reduces the low-frequency grounding impedance by a factor of two if this connection is performed by an insulated conductor. This reduction is greater if a bare conductor is used because more current is injected into the soil. As the frequency increases, the effect of the adjacent grounding system becomes gradually negligible and the impedance value tends to the one of the single wind turbine grounding system. The frequency at which this occurs is higher for bare conductors and high-resistivity soils.
- When the grounding systems are connected through a bare conductor, the GPR peak reduction is essentially due to the interconnecting conductor, and the adjacent grounding system is responsible only for a decrease of the GPR tail.
- When the grounding systems are connected through an insulated conductor, the GPR peak reduction is basically due to the current that is partly diverted to the adjacent tower and partly drained to charge the insulation capacitance. For first stroke currents, the adjacent grounding system also contributes to the GPR peak decrease, **mainly for shorter distances between wind turbines.**

## VI. APPENDIX

The per-unit-length impedance  $Z$  and admittance  $Y$  of a perfectly-conducting underground conductor covered by an insulating layer are given by [23]

$$Z = Z_e + Z_g \quad (\text{A1})$$

$$Y = \frac{j\omega C \times Y_g}{j\omega C + Y_g} \quad (\text{A2})$$

In (A1),  $Z_e = j\omega L$  is the external impedance due to the magnetic field within the insulation and  $Z_g$  is the ground return impedance. In (A2),  $C$  is the insulation capacitance and  $Y_g$  is the ground admittance. The per-unit-length inductance and capacitance due to the insulation are calculated using [23]

$$L = \frac{\mu_0}{2\pi} \ln\left(\frac{b}{a}\right) \quad (\text{A3})$$

$$C = \frac{2\pi\epsilon_{ins}}{\ln\left(\frac{b}{a}\right)} \quad (\text{A4})$$

where  $a$  and  $b$  are respectively the inner and outer insulation radius,  $\epsilon_{ins}$  is the insulation permittivity, and  $\mu_0$  is vacuum permeability. In this paper,  $a = 5.8$  mm,  $b = 7.6$  mm, and  $\epsilon_{ins} = 2.3\epsilon_0$ .

The ground return impedance is computed using Sunde's expression, which is given by [22]

$$Z_g = \frac{j\omega\mu_0}{2\pi} \left[ \frac{K_0(\gamma_g r_0) - K_0(2\gamma_g h) + \int_0^\infty \frac{\exp(-2h\sqrt{\lambda^2 + \gamma_g^2})}{|\lambda| + \sqrt{\lambda^2 + \gamma_g^2}} \cos(\lambda r_0) d\lambda}{2} \right] \quad (\text{A5})$$

where  $\gamma_g = \sqrt{j\omega\mu_0(\rho_g^{-1} + j\omega\epsilon_g)}$  is the ground propagation constant,  $r_0 = b$ ,  $h$  is the burial depth of the conductor, and  $K_0(\cdot)$  is Bessel's function of second kind and order zero.

The ground admittance is obtained from [23]

$$Y_g \approx \frac{Y_g^2}{Z_g} \quad (\text{A6}).$$

## VII. REFERENCES

- [1] J. Lee and F. Zhao. *Global Wind Report 2019*, Global Wind Energy Council: Brussels, Belgium, 2020.
- [2] International Electrotechnical Commission (IEC), *IEC 61400: Wind energy generation systems – Part 24: Lightning protection*. Geneva, Switzerland, 2019.
- [3] T. Soerensen, "Lightning protection of wind turbines, Chapter 14," in *Lightning Protection*, 1st ed., London: IET, 2010, pp. 681–722.
- [4] F. Rachidi et al., "A Review of Current Issues in Lightning Protection of New-Generation Wind-Turbine Blades," *IEEE Trans. Ind. Electron.*, vol. 55, no. 6, pp. 2489–2496, Jun. 2008.
- [5] K. Yamamoto, S. Yanagawa, K. Yamabuki, S. Sekioka, and S. Yokoyama, "Analytical Surveys of Transient and Frequency-Dependent Grounding Characteristics of a Wind Turbine Generator System on the Basis of Field Tests," *IEEE Trans. Power Deliv.*, vol. 25, no. 4, pp. 3035–3043, Oct. 2010.
- [6] B. Markovski, L. Greev, and V. Arnautovski-Toseva, "Transient characteristics of wind turbine grounding," in *2012 International Conference on Lightning Protection (ICLP)*, 2012, pp. 1–6.

- [7] V. T. Kontargyri, I. F. Gonos, and I. A. Stathopoulos, "Study on Wind Farm Grounding System," *IEEE Trans. Ind. Appl.*, vol. 51, no. 6, pp. 4969–4977, Nov. 2015.
- [8] D. S. Gazzana, A. Smorgonskiy, N. Mora, A. Šunjerga, M. Rubinstein, and F. Rachidi, "An experimental field study of the grounding system response of tall wind turbines to impulse surges," *Electr. Power Syst. Res.*, vol. 160, pp. 219–225, Jul. 2018.
- [9] R. Alipio, D. Conceição, A. De Conti, K. Yamamoto, R. N. Dias, and S. Visacro, "A comprehensive analysis of the effect of frequency-dependent soil electrical parameters on the lightning response of wind-turbine grounding systems," *Electr. Power Syst. Res.*, vol. 175, p. 105927, Oct. 2019.
- [10] S. Sekioka, H. Otoguro, and T. Funabashi, "A Study on Overvoltages in Windfarm Caused by Direct Lightning Stroke," *IEEE Trans. Power Deliv.*, vol. 34, no. 2, pp. 671–679, Apr. 2019.
- [11] M. R. Ahmed and M. Ishii, "Effectiveness of interconnection of wind turbine grounding influenced by interconnection wire," in *2012 International Conference on Lightning Protection (ICLP)*, 2012, pp. 1–6.
- [12] B. Markovski, L. Grcev, V. Arnautovski-Toseva, and M. Kacarska, "Transient performance of interconnected wind turbine grounding systems," *Przegľad Elektrotechniczny*, vol. 1, no. 6, pp. 74–77, Jun. 2015.
- [13] A. Sunjerga, Q. Li, D. Poljak, M. Rubinstein, and F. Rachidi, "Isolated vs. Interconnected Wind Turbine Grounding Systems: Effect on the Harmonic Grounding Impedance, Ground Potential Rise and Step Voltage," *Electr. Power Syst. Res.*, vol. 173, pp. 230–239, Aug. 2019.
- [14] R. Alipio, M. T. Correia de Barros, M. A. O. Schroeder, and K. Yamamoto, "Analysis of the lightning impulse and low-frequency performance of wind farm grounding systems," *Electr. Power Syst. Res.*, vol. 180, p. 106068, Mar. 2020.
- [15] R. Alipio and S. Visacro, "Modeling the Frequency Dependence of Electrical Parameters of Soil," *IEEE Trans. Electromagn. Compat.*, vol. 56, no. 5, pp. 1163–1171, Oct. 2014.
- [16] Working Group C4.33, *Impact of soil-parameter frequency dependence on the response of grounding electrodes and on the lightning performance of electrical systems (WG C4.3)*. CIGRE, 2019.
- [17] A. De Conti and S. Visacro, "Analytical Representation of Single- and Double-Peaked Lightning Current Waveforms," *IEEE Trans. Electromagn. Compat.*, vol. 49, no. 2, pp. 448–451, May 2007.
- [18] K. Berger, R. B. Anderson, and H. Kroninger, "Parameters of lightning flashes," *Electra*, no. 80, pp. 223–237, 1975.
- [19] J. C. Salari and C. Portela, "A Methodology for Electromagnetic Transients Calculation—An Application for the Calculation of Lightning Propagation in Transmission Lines," *IEEE Trans. Power Deliv.*, vol. 22, no. 1, pp. 527–536, Jan. 2007.
- [20] S. Visacro and A. Soares, "HEM: A Model for Simulation of Lightning-Related Engineering Problems," *IEEE Trans. Power Deliv.*, vol. 20, no. 2, pp. 1206–1208, Apr. 2005.
- [21] A. Ametani, "A General Formulation of Impedance and Admittance of Cables," *IEEE Trans. Power Appar. Syst.*, vol. PAS-99, no. 3, pp. 902–910, May 1980.
- [22] E. D. Sunde, *Earth Conduction Effects in Transmission Systems*. New York: Dover Publications, 1968.
- [23] F. M. Tesche, M. V. Ianoz, and T. Karlsson, *EMC Analysis Methods and Computational Models*. New York: Wiley, 1997.
- [24] N. Theethayi, Y. Baba, F. Rachidi, and R. Thottappillil, "On the Choice Between Transmission Line Equations and Full-Wave Maxwell's Equations for Transient Analysis of Buried Wires," *IEEE Trans. Electromagn. Compat.*, vol. 50, no. 2, pp. 347–357, May 2008.
- [25] C. R. Paul., *Analysis of multiconductor transmission lines*, 2nd ed. John Wiley & Sons, Inc., 2008.
- [26] L. Grcev, "Impulse Efficiency of Ground Electrodes," *IEEE Trans. Power Deliv.*, vol. 24, no. 1, pp. 441–451, Jan. 2009.
- [27] R. Alipio and S. Visacro, "Impulse Efficiency of Grounding Electrodes: Effect of Frequency-Dependent Soil Parameters," *IEEE Trans. Power Deliv.*, vol. 29, no. 2, pp. 716–723, Apr. 2014, doi: 10.1109/TPWRD.2013.2278817.